DIMENSION REDUCTION USING THE INVERSE STAMPING METHOD

JAROMIR KASPAR[1], MARCEL SVAGR[2], PETR BERNARDIN[2], VACLAVA LASOVA[2], OTOMAR SEDIVY[1]

[1]Mubea, spol. s.r.o., Innovation Department

[2]University of West Bohemia in Pilsen, Faculty of Mechanical Engineering, Department of Machine Design

DOI: 10.17973/MMSJ.2021_10_2021089

Jaromir.Kaspar@mubea.com

The aim of this work is to improve the inverse stamping method and increase its robustness. The first, crucial step of inverse stamping is the reduction of the three-dimensional part into a two-dimensional flat plane. There are several methods for reducing the dimension. These are geometrical methods, methods based on graph theory and stochastic methods. We examine the last two methods because of their reliability. These methods can even be used for geometrically complex structures which include holes, hooks and walls perpendicular to the flat plane. An algorithm which combines several methods for dimension reduction is proposed for use for a wide range of parts. Deep drawing is a widely used technology in the automotive industry and inverse stamping is a useful development tool.

KEYWORDS

Inverse stamping, finite element method, graph theory, stochastic method, dimensional reduction

1 INTRODUCTION

Inverse stamping [Batoz 2004, Naceur 2004] is commonly used by engineers for many tasks. It can be used for designing technological processes and is also useful for designing stamped parts. Inverse stamping has three main steps. In the first step, the three-dimensional (3D) part is projected into a flat plane, i.e. the shape is reduced from three to two dimensions. The projected part is used as the initial input for the second step. Two dimensional (2D) finite element analysis (FEA) is used in this step for iterative improvement of the result of the first step. If the convergence criterion is fulfilled, i.e. the initial flat shape is known, the third step is completed and the results are evaluated based on the initial flat shape and the final 3D shape. For a 2D FEA plane stress problem [Zienkiewicz 2005] it is important that normal orientation of all the elements is the same and the area of all the elements is non-zero. Zero area elements are typical for parts which have walls perpendicularly oriented to the projection plane. Some geometrical approaches solve this issue using a step-by-step projection of the elements to the flat plane with subsequent connection. This algorithm is suitable for moderately smooth parts without holes. Different methods must be used for more geometrically complex parts.

2 DIMENSION REDUCTION

The first step of inverse stamping is dimension reduction. A 3D FEA mesh is reduced to a 2D mesh. Methods for this task are based on graph theory or the stochastic approach. These methods were originally developed, inter alia, for analysing multidimensional data and machine learning. The dimension is reduced during the analysis respecting the properties of the original data set. Dimension reduction methods are described in sections 2.1, 2.2, 2.3 and 2.4.

2.1 *Locally Linear Embedding (LLE)*

In the first step of the LLE method, the specific number of the closest adjacent points (or nodes) is found and then a graph (a structure defined by a set of vertices and a set of edges) is compiled [Cada 2004]. The graph is represented by weight corresponding with the distance between adjacent points [Roweis 2000]. The weight matrix *[W]* is used for spatial reconstruction of the points with the reduced dimension. There are several methods of LLE. If the conventional method [Roweis 2000] is used, then some weights can be zero, which leads to ambiguous solutions. Therefore, conventional LLE uses the following procedure:

a) Weighted adjacency matrix *[Z]* [Cada 2004] for point *i* is assembled.
b) Matrix *[C]* is calculated as $[C]=[Z][Z]^T$.
c) Diagonal of *[C]* matrix is modified by adding regularization term *r*, i.e. *[S]=[C]+r[I]*, where *[I]* is identity matrix.
d) Weights *{w}* are calculated as a solution of equation *[S]{w}={i}*, where *{i}* is column matrix of ones.
e) Weights *{w}* of point *i* are added to global weight matrix *[W]*

Due to the issue of choosing a regularization term *r*, the modified LLE (MLLE) [Zhang 2006] and Hessian LLE [Donoho 2003] were developed. LLE methods also include the Local Tangent Space Alignment (LTSA) method [Wang 2012, Hongyu 2005]. LTSA does not use the distances of adjacent nodes to represent local properties, but instead uses local tangent spaces. This is shown in Figure 1, where local tangent spaces are represented by solid lines and the original shape is represented by the dashed line.

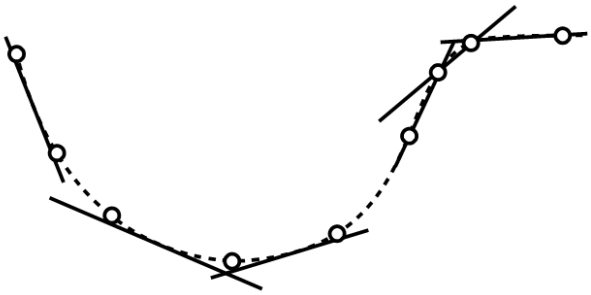

Figure 1. Local tangent spaces

Determining the adjacent points (specifically their number) is difficult, especially if the part includes protrusions (e.g. a hook-shaped substructure). A 3D mesh of a part with a protrusion (1) is shown in Figure 2.

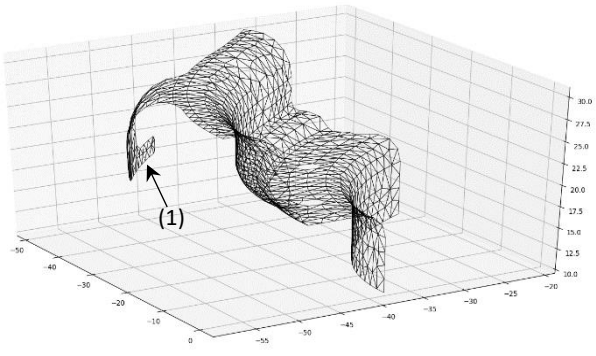

Figure 2. 3D mesh with hook-shaped protrusion

The required 2D projection is shown in Figure 3.

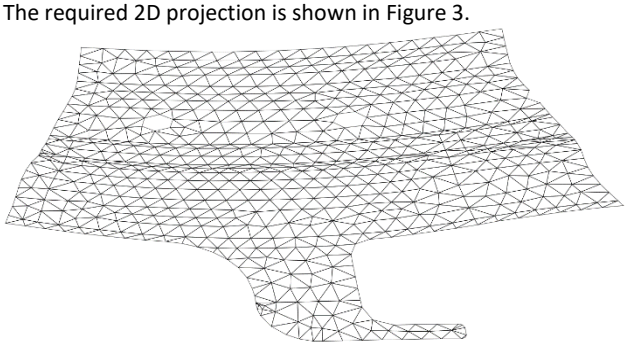

Figure 3. Required 2D projection

Using the conventional LLE method with the number of adjacent points set to five, a significant deformation of the hook-shaped protrusion (2) occurs (see Figure 4).

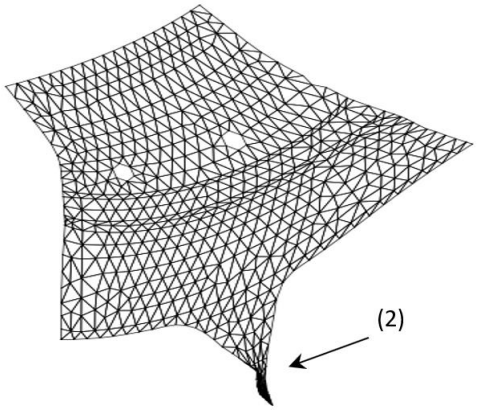

Figure 4. LLE with number of neighbouring points set to five

Increasing the number of adjacent points to fifteen leads to the flipping (3) of the hook-shaped protrusion (see Figure 5).

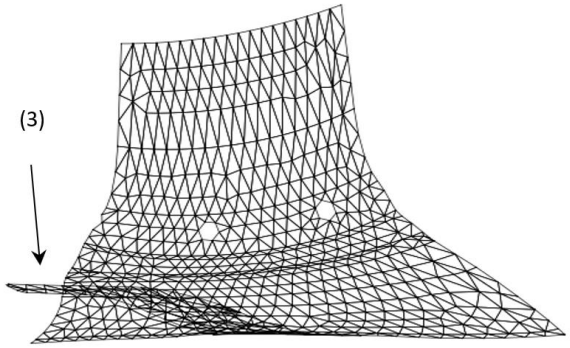

Figure 5. Flipping of the hook-shaped protrusion

2.2 *Isomap*

The name of this method is derived from the phrase 'isometric mapping' [Tanenbaum 2000, Choi 2007]. The first step is the same as in the previous LLE method (the determination of the adjacent points). Then, the weighted adjacency matrix *[M]* is assembled. The geodesic distance between all pairs of points is calculated by using matrix *[M]* and the results are entered in to matrix *[G]*. With the help of the decomposition of *[G]* into eigenvalues and eigenvectors, the set of points in space is found (respecting the reduced dimension).

2.3 *t-SNE*

The t-SNE [van der Maaten 2008] method is based on Stochastic Neighbour Embedding (SNE). The first step of SNE is determining the neighbouring points for the whole part and the following evaluation of their distances. This task is performed using an internal algorithm. The distances are used for assembling the asymmetrical probability matrix *[P]*. The element of *[P]* matrix p_{ij} reflects the probability that the point indexed by *i* is a neighbour of the point indexed by *j*. SNE uses Gaussian probability distribution. If the density of points is higher, then the standard deviation of Gaussian distribution is lower. In the next step, the initial guess in the space with the reduced dimension is randomly determined and a probability matrix with a constant standard deviation is assembled. The difference between both probability distributions is iteratively minimized. This increases the calculation time (compared with LLE methods and Isomap). t-SNE uses Student's distribution (also called t-distribution), instead of Gauss distribution and uses a symmetrical probability matrix *[P].*

2.4 **Spectral Embedding (SE)**

The first step of the SE approach [Belkin 2002] is the same as in the previous methods (the determination of the adjacent points and assembly of a graph). The edges of the graph are evaluated, while weights are stored in matrix *[W]*. Matrix *[W]* is used to calculate the Laplacian matrix *[L]* [Cada 2004]. If λ_i are eigenvalues of *[L]* in ascending order and $\{v_i\}$ are corresponding eigenvectors, then the rows of matrix *[Y]* in equation 1 are coordinates of points in space with dimension *k*. The total number of points is *n*.

$$[Y] = [\{v_2\} \dots \{v_{k+1}\}] \in \mathbb{R}^{n \times k} \quad (1)$$

3 INVERSE STAMPING ALGORITHM

LLE methods, Isomap, t-SNE and SE allow the dimension to be reduced and the acquisition of the projected nodal coordinates. When the initial guess is known, the second and third steps can follow. The second step has the following substeps [Farahani 2014], [Azizi 2008]:

a) Each element is unfolded
b) Nodal displacements $\{\Delta u_e\}$ of each element are calculated as the difference between unfolded and projected nodal coordinates. Nodal forces are calculated.
c) Global stiffness matrix *[K]* and external forces vector *{F}* are assembled. Increment of nodal displacements *{Δu}* are calculated as a solution of linear equations system *[K]{Δu}=[F]*
d) Nodal coordinates are updated by adding *{Δu}*
e) Material properties are updated
f) After the convergence criterion is fulfilled, the second step is stopped. Otherwise, the algorithm goes to substep b).

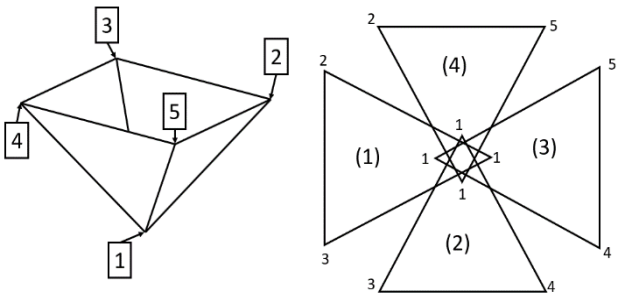

Figure 6. Elements unfolding

Elements are unfolded in substep a) [Shirin 2014] . The 3D mesh (left) and its unfolded elements (right) are shown in Figure 6. The unfolded mesh is discontinuous. Node 5 in Figure 6 is a

member of the unfolded element (3) and is not coincident with node 5 of the unfolded element (4). The unfolded mesh is created by rotating the position vectors of its nodes by a specific angle (described in equation 2).

$$\propto = \arccos(\{n\}\{k\}) \tag{2}$$

Symbol *{n}* denotes the normal vector of the 3D element and *{k}* is the normal vector of the target flat plane. The transformation matrix for unfolding is described in equation 3.

$$[R] = \begin{bmatrix} m_1^2\mu + cos\alpha & m_1m_2\mu - m_3sin\alpha & m_1m_3\mu + m_2sin\alpha \\ m_1m_2\mu + m_3sin\alpha & m_2^2\mu + cos\alpha & m_2m_3\mu - m_1sin\alpha \\ m_1m_3\mu - m_2sin\alpha & m_2m_3\mu + m_1sin\alpha & m_3^2\mu + cos\alpha \end{bmatrix}, \tag{3}$$

where μ, m_1, m_2 and m_3 are described in equations 4 and 5.

$$\mu = 1 - cos\alpha \tag{4}$$

$$[m_1 \quad m_2 \quad m_3]^T = \frac{1}{\|\{n\}\times\{k\}\|}\{n\} \times \{k\} \tag{5}$$

The centre of rotation of the element is equal to the geometric element centre. During substep c), the global stiffness matrix *[K]* and global vector of external forces *{F}* is assembled. The stiffness matrix $[K_e]$ of each planar triangular element is calculated first. Matrix $[K_e]$ is given by equation 6.

$$[K_e] = tA[B]^T[D][B], \tag{6}$$

where *t* is element thickness, *A* is area of the element and the material stiffness matrix *[D]* is in equation 7.

$$[D] = \frac{E(1+a)}{1+2a}\begin{bmatrix} 1+a & a & 0 \\ a & 1+a & 0 \\ 0 & 0 & 0.5 \end{bmatrix} \tag{7}$$

Symbol *a* denotes normal anisotropy. If stress is zero, then *E* is Young's modulus. If stress is non-zero, *E* is the ratio of the equivalent stress to the equivalent strain (see equation 8).

$$E = \frac{\bar{\sigma}}{\bar{\varepsilon}} \tag{8}$$

Strain-displacement matrix *[B]* (used in equation 6) is in equation 9.

$$[B]^T = \frac{1}{\det[J]}\begin{bmatrix} y_2 - y_3 & 0 & x_3 - x_2 \\ 0 & x_3 - x_2 & y_2 - y_3 \\ y_3 - y_1 & 0 & x_1 - x_3 \\ 0 & x_1 - x_3 & y_3 - y_1 \\ y_1 - y_2 & 0 & x_2 - x_1 \\ 0 & x_2 - x_1 & y_1 - y_2 \end{bmatrix}, \tag{9}$$

where x_i and y_i for *i=1, 2, 3* are current nodal coordinates in *x*-direction and *y*-direction. The Jacobian matrix *[J]* is described in equation 10.

$$[J] = \begin{bmatrix} x_1 - x_3 & y_1 - y_3 \\ x_2 - x_3 & y_2 - y_3 \end{bmatrix} \tag{10}$$

If $[K_e]$ is known for each element, then the standard procedure for assembling *[K]* is used. External forces acting on each element are calculated according to equation 11.

$$\{F_e\} = [K_e]\{\Delta u_e\} \tag{11}$$

The global external force vector *{F}* is assembled based on $\{F_e\}$. Material properties are updated in substep e). Material stiffness is given by the local stress-strain relationship (see equation 8). Equivalent strain and stress are calculated based on the difference between the 2D element and the 3D element. Equivalent strain [Farahani 2014] is calculated based on equation 12.

$$\bar{\varepsilon} = \sqrt{\frac{2}{3}F\left(B\varepsilon_{xx}^2 + 2\varepsilon_{xx}\varepsilon_{yy} + C\varepsilon_{xx}^2 + 2D\varepsilon_{xy}^2\right)}, \tag{12}$$

where constants *F*, *B*, *C*, *D* are described in equations 13-15.

$$F = \frac{a(2+a)}{1+2a} \tag{13}$$

$$B = C = \frac{1+a}{a} \tag{14}$$

$$D = \frac{1}{a} \tag{15}$$

Stress-strain curve is approximated based on equation 16.

$$\bar{\sigma} = m\bar{\varepsilon}^g \tag{16}$$

Constants *m* and *g* in equation 16 were estimated based on measurement. Components of strain used in equation 12 are described in equation 17

$$\begin{bmatrix} \varepsilon_{xx} \\ \varepsilon_{yy} \\ \varepsilon_{xy} \end{bmatrix} = \begin{bmatrix} ln\lambda_1 cos^2\Theta + ln\lambda_2 sin^2\Theta \\ ln\lambda_1 sin^2\Theta + ln\lambda_2 cos^2\Theta \\ (ln\lambda_1 - ln\lambda_2)sin\Theta cos\Theta \end{bmatrix}, \tag{17}$$

where λ_1, λ_2 are given by equation 18.

$$\begin{bmatrix} \lambda_1 \\ \lambda_2 \end{bmatrix} = \begin{bmatrix} \left((1/2)(C_{11} + C_{22}) + (1/2)((C_{11} - C_{22})^2 + 4C_{12}^2)^{1/2}\right)^{-1/2} \\ \left((1/2)(C_{11} + C_{22}) - (1/2)((C_{11} - C_{22})^2 + 4C_{12}^2)^{1/2}\right)^{-1/2} \end{bmatrix} \tag{18}$$

Angle Θ used in equation 17 is described in equation 19.

$$\Theta = arctan\left(\frac{\lambda_1^{-2} - C_{11}}{C_{12}}\right) \tag{19}$$

Elements of symmetric matrix *[C]*, equation 23, are shown in equations 20-22.

$$C_{11} = \frac{1}{(h_{2y}h_{3x} - h_{2x}h_{3y})^2}\left(h_{3y}^2L_2 + h_{2y}^2L_3 - (L_2 + L_3 - L_1)h_{2y}h_{3y}\right) \tag{20}$$

$$C_{22} = \frac{1}{(h_{2y}h_{3x} - h_{2x}h_{3y})^2}\left(h_{3x}^2L_2 + h_{2x}^2L_3 - (L_2 + L_3 - L_1)h_{2x}h_{3x}\right) \tag{21}$$

$$C_{12} = \frac{1}{(h_{2y}h_{3x} - h_{2x}h_{3y})^2}\left(-h_{3x}h_{3y}L_2 - h_{2x}h_{2y}L_3 + (1/2)(L_2 + L_3 - L_1)\left(h_{2y}h_{3x} + h_{2x}h_{3y}\right)\right) \tag{22}$$

$$[C] = \begin{bmatrix} C_{11} & C_{12} \\ C_{12} & C_{22} \end{bmatrix} \tag{23}$$

Vectors *{h2}* and *{h3}*, (used in equations 20, 21, 22) have the same orientation as the edges of the 3D element (see Figure 7) given by nodal coordinates x_i, y_i, z_i.

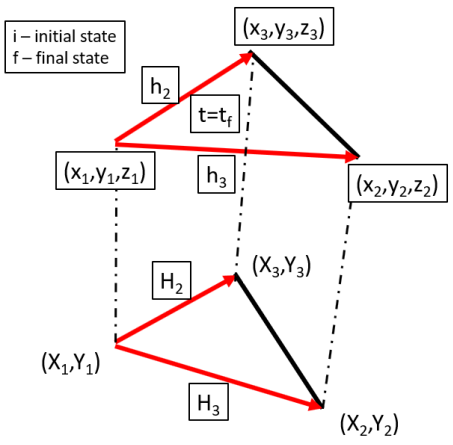

Figure 7. 2D and 3D elements

L_1, L_2, L_3 are the lengths of the 2D element edges given by nodal coordinates X_i, Y_i. The third step of inverse stamping includes the

final evaluation of interesting values, specifically plastic strain, or residual stress.

4 MODELLING THE STAMPED PARTS

There are several ways to evaluate the stamped parts [Qattawi 2014]. These differ in the degree of accuracy, the complexity of the model and the time required to calculate and prepare the model. It is possible to use a complex calculation in the appropriate solver of FEM software. Another option for calculation uses the simplified tools included in commercial programs, called “Inverse stamping”. Some open source software tools can be further customized. Another possibility is to develop a program which is completely or partially separate from the commercial program.

4.1 Utilization of the complex calculation in commercial FEM solvers

The prediction of the behaviour of the formed part is conditioned by the knowledge of the shape of the forming tool. Then it is possible to calculate the resulting stress and the resulting deformation. Therefore, this method cannot be called “Inverse stamping”. When designing specific parts, the procedure is often reversed. The final shape of the part is known (based on the designed model) and the main task is to determine the initial shape (flat plane) of the part and the residual stresses, or relative deformation. This procedure is much more complicated, depending on the number of forming operations (or tools) that are necessary to obtain the final shape of the part. The time required to create the model depends on the shape complexity of the part, as well as the time required for the calculation itself. Compared with other variants used for predicting the behaviour of stamped parts, this method is one of the most time-consuming processes, but it provides highly accurate results.

4.2 Utilization of the simplified software tool – “NX Analyze Formability – One-step”

Simplified tools can be used to predict the behaviour of a part in the early phase of the design process. These tools must meet time and accuracy requirements. They are usually called single-purpose modules that are implemented in commercial modelling software. These modules either contain several commands or are based on the complete source code. Their main advantage is they can be used to perform a preliminary calculation of the stamped parts very simply and quickly. The main disadvantage of these tools is their rigidity, or inability to modify the source code, limited parameter options, or limited suitability for parts with shape diversity. A case study was done to demonstrate these positives and negatives.

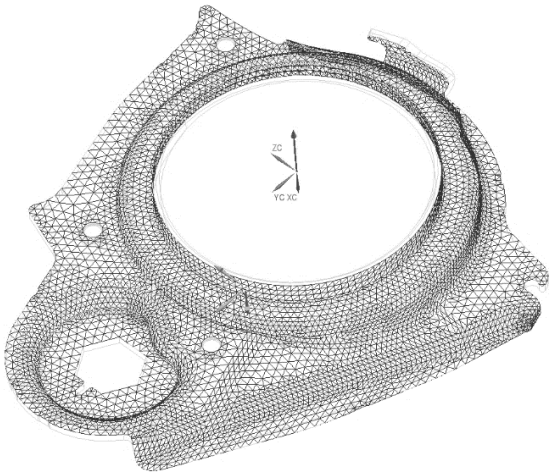

Figure 8. 3D mesh of the part before performing the simulation in the module "NX Analyze Formability - One-step"

The module "NX Analyze Formability - One-step" was used for specific parts (see Figure 8 and Figure 9). The results show a significant deformation of the mesh that no longer meets the condition of mesh quality. These mesh errors occur for parts in which the normal of the stamped surface forms an angle greater than 90° to the base surface (unformed).

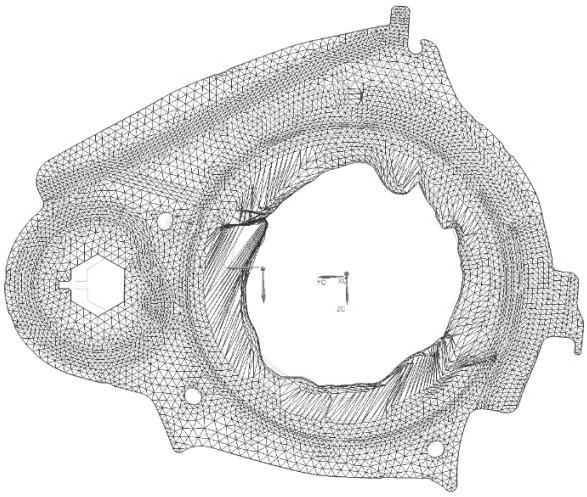

Figure 9. 3D mesh of the stamped part after performing the simulation in the module "NX Analyze Formability - One-step"

The applicability of the “NX Analyze Formability - One-step” module for a specific part (Figure 8 and Figure 9) is summarized below:

- The tool is suitable for simplified analysis of stamped parts made of sheet metal with constant thickness, made of different materials.
- This method uses the flat plane without intermediate steps (partial unforming and therefore the technological process (sequence of forming operations) is not included in the calculation.
- Significant deformation, even destruction of the mesh elements, was determined for some parts. These elements did not meet the mesh quality requirements and the resulting stress, displacement and change in thickness was not correct for these parts. In this particular case this was due to the shape of the part, where the normal of the model surface is rotated by more than 90 ° relative to the normal of the unfolded surface.

- The condition of the minimum element size (depending on the sheet thickness) is very limiting.
- Analysis of the spring-back of the part can only be performed using the partial unfolding process. The analysis of spring-back is not feasible without knowledge of the technological process, which is a significant limitation.
- Analysis using the basic function of the module ("Entire Uniform") is fast. Its accuracy (resulting stress) depends on the suitability of the part for forming (mesh quality).

4.3 The creation of a separate algorithm

Another option is to develop a standalone application, where the algorithm is completely or partially outside the commercial program. It allows a simplified calculation to be done, or to adapt it for a specific type of part. When creating a standalone algorithm for inverse stamping (or modifying an existing algorithm) it is necessary to choose a method for predicting the flat shape of the part. The following section deals with this issue.

5 COMPARISON OF PROJECTION METHODS

Projection methods applicable for dimension reduction were briefly described in sections 2.1, 2.2, 2.3, 2.4. The suitability of these methods was verified using two parts. Part A is a stabilizer clamp (see Figure 10), whose mesh includes 1154 nodes.

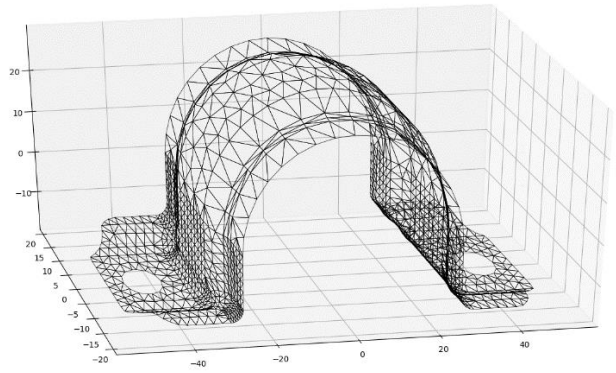

Figure 10. Part A: Stabilizer clamp

Part B is a belt tensioner lever arm (see Figure 11), whose mesh includes 4785 nodes.

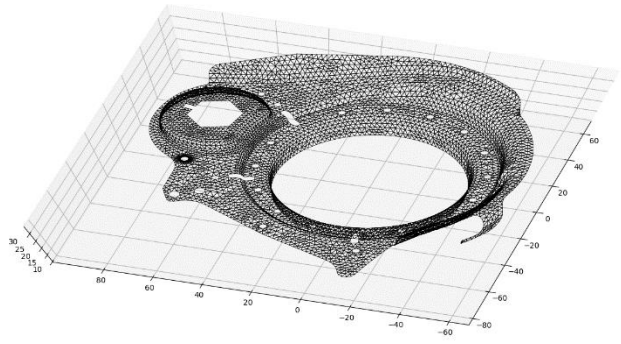

Figure 11. Part B: Lever arm

Both parts were manufactured using stamping technology. They include holes and walls perpendicularly oriented to the projection plane. All the methods were tested with different settings. If all the mesh elements are oriented in the same direction (after completing the dimension reduction), then the method (including settings) is applicable. During the calculation the number of improving iterations in the second step of the inverse stamping procedure is monitored, as well as the computation time. The suitability of a method depends on the number of iterations. Each setting is verified three times and the average values are presented. The Hessian LLE method needs at least six adjacent nodes if a two-dimensional reduced space is used. All the methods use from six to forty adjacent nodes.

6 RESULTS AND DISCUSSION

All the methods were successfully used for part A except the SE method. The conventional LLE method was not successful for many settings. Other methods were reliable with minor exceptions, see Figure 12. The t-SNE method is not dependent on the number of neighbouring nodes and the results are constant (in terms of this number).

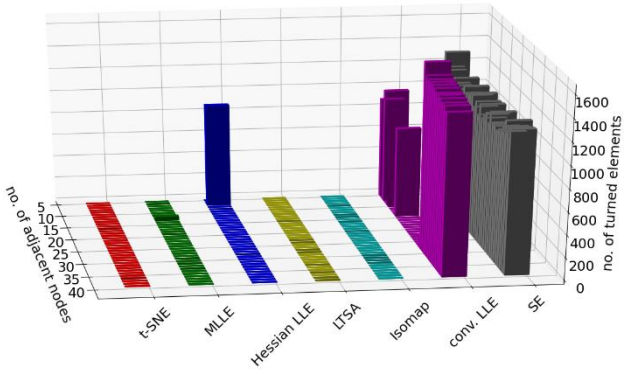

Figure 12. Number of turned elements, part A

Results for part B are shown in Figure 13. Due to the more complex geometry, SE, conventional LLE and Isomap methods failed. Hessian LLE and LTSA methods allowed the calculation of an appropriate initial guess, but the number of adjacent nodes has to be lower than twenty. The MLLE method respects a range from ten to twenty.

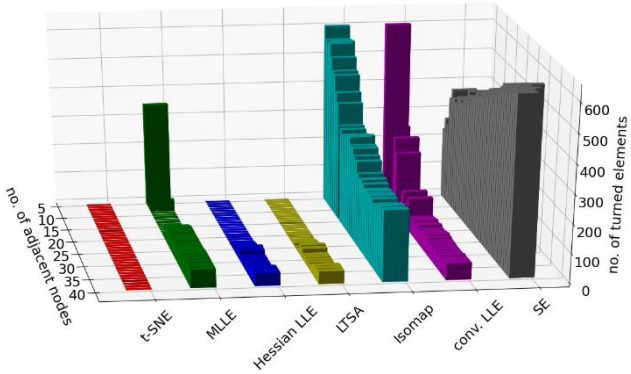

Figure 13. Number of turned elements, part B

The calculation time of the inverse stamping algorithm is influenced by the rate of reduction of this method and by the number of improvement iterations in the second step. The longer calculation time for dimensional reduction is compensated by the lower number of the improvement iterations. The number of required iterations for part A is shown in Figure 14. Only applicable configurations were included. The best results were obtained using the Isomap method after seven iteration steps, followed by the t-SNE method with eight iteration steps. Other configurations are more time consuming in relation to the number of iteration steps.

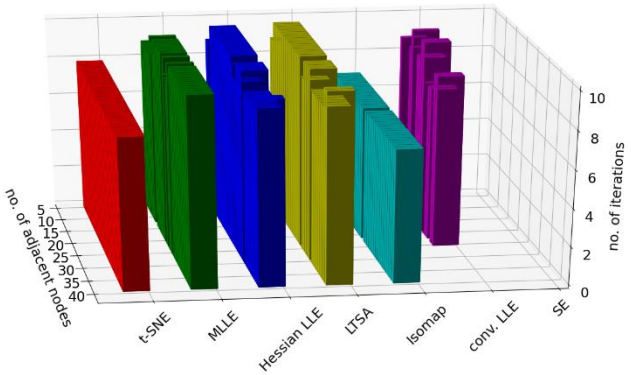

Figure 14. Number of improvement iterations, part A

The number of iteration steps for part B is shown in Figure 15. The best results were obtained by t-SNE after six iteration steps.

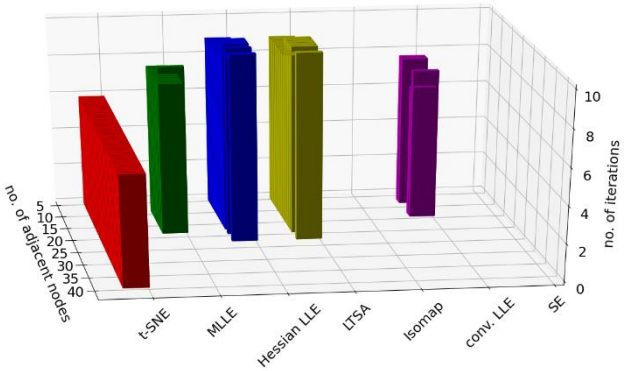

Figure 15. Number of improvement iterations, part B

Figure 16 describes the calculation time required for dimension reduction of part A. The projection time is usually shorter than 1 second, except for t-SNE which is about 6 seconds.

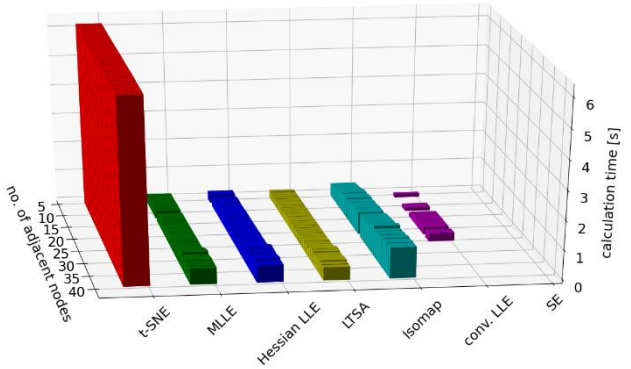

Figure 16. Calculation time, part A

Calculation time of part B projection has a similar character. t-SNE is more time consuming than the others (see Figure 17), but this method is preferred.

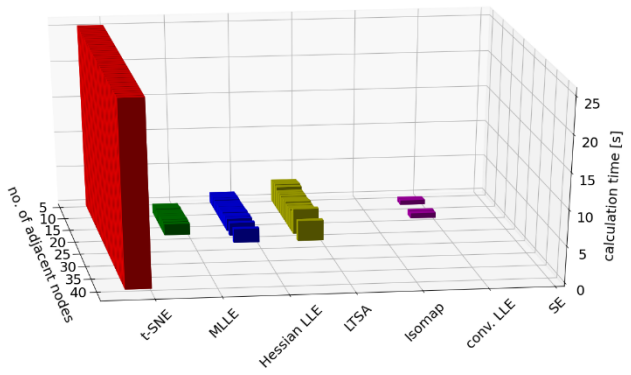

Figure 17. Calculation time, part B

The main reason for this is its high reliability and small number of required improvement iteration steps. The determination of the number of neighbouring nodes is not required by the t-SNE method, which means it is more user-friendly. A robust algorithm based on the presented data is proposed for dimension reduction. The algorithm includes the following methods: t-SNE, MLLE, Hessian LLE and LTSA.

The algorithm has the following steps:

a) t-SNE method is used. After reaching the same orientation of all elements, the algorithm ends.
b) Number of neighbouring nodes is initialized to six, z=*6*.
c) Method MLLE is used with parameter *z*. If all elements reach the same orientation, algorithm ends.
d) Method Hessian LLE is used with parameter *z*. Algorithm ends if successful.
e) LTSA method is used with parameter *z*. After reaching the same orientation of all elements, the algorithm ends. Otherwise, *z* is increased by one and algorithm goes to step c).

The algorithm can be used for various shapes, from simple components to geometrically complex parts, including holes and perpendicular walls. Robustness of the algorithm is demonstrated in table 1, where there are results achieved with the proposed algorithm. The algorithm was successful in every case. If the amount of mesh nodes was too low, then t-SNE method failed and another method had to be used. For this reason the algorithm contains methods from LLE group.

Number of mesh nodes	used method (number of adjacent nodes)	Calculation time [s]	note
75	MLLE(6)	0.57	t-SNE failed
224	MLLE(6)	1.18	t-SNE failed
480	MLLE(6)	2.49	t-SNE failed
686	t-SNE()	3.83	
766	t-SNE()	3.70	
984	t-SNE()	4.82	
1154	t-SNE()	6.20	
4785	t-SNE()	26.34	

Table 1. Proposed algorithm results

7 CONCLUSIONS

Several methods of dimension reduction were described, including the inverse stamping algorithm. Reduction methods were fully integrated into the inverse stamping process. All the methods were verified by comparing their important characteristics. Any reduction method can be used in inverse stamping if all the mesh elements are oriented in the same direction. This essential requirement was not fulfilled by the SE method for any settings. The Isomap method failed for geometrically complex parts. The conventional LLE method showed poor performance due to the limited setup options. Other methods from the LLE group achieved good results, as did the t-SNE method. The aim of this research was to increase the robustness of the inverse stamping method. Based on the presented study, an algorithm for dimension reduction was proposed. The algorithm includes t-SNE, MLLE, Hessian LLE and LTSA methods. This innovative solution can be utilized for a wide range of parts (including holes, hook-shaped protrusions, or walls perpendicular to the projection plane). The algorithm is characterised by high robustness.

ACKNOWLEDGMENTS

This article has been prepared under project FV40348 'Parts development with advanced numerical simulation tools for the AUTOMOTIVE' under the auspices of the Ministry of Industry and Trade of the Czech Republic.

REFERENCES

[Azizi 2008] Azizi, R. and Assempour, A. Applications of linear inverse finite element method in prediction of the optimum blank in sheet metal forming. Materials and Design, 2008, Vol. 29, pp 1965-1972

[Batoz 2004] Batoz, J.L. et al. Sheet Metal Stamping Analysis and Process Design based on the Inverse Approach. AIP Conference Proceedings. 907, 2004. DOI: 1448-1453. 10.1063/1.2729719

[Belkin 2002] Belkin, M. and Niyogi, P. Laplacian Eigenmaps for Dimensionality Reduction and Data Representation. Neural Computation, June 2003, Vol. 15, No. 6, pp 1373-1396

[Cada 2004] Cada, R. et al. Discrete mathematics. Pilsen: ZCU in Pilsen, 2004. ISBN 80-7082-939-7 (in Czech)

[Choi 2007] Choi, H. et al. Robust kernel Isomap. Pattern Recognition. 40. 853-862. DOI: 10.1016/j.patcog.2006.04.025.

[Donoho 2003] Donoho, D.L. and Grimes, C. Hessian eigenmaps: Locally linear embedding techniques for high-dimensional data. PNAS, May 2003, Vol. 100, No. 10, pp 5591-5596

[Farahani 2014] Farahani, M.K. et al. Development of an inverse element method with an initial guess of linear unfolding. Finite Elements in Analysis and Design, 2014, Vol. 79, pp 1-8

[Hongyu 2005] Hongyu,L. et al. Supervised Local Tangent Space Alignment for Classification. Conference: IJCAI-05, Proceedings of the Nineteenth International Joint Conference on Artificial Intelligence, Edinburgh, Scotland, UK, July 30-August 5, pp. 1620-1621, 2005.

[Naceur 2004] Naceur, H. et al. The inverse approach for the design of sheet metal forming parameters to control springback effects. ECCOMAS 2004 - European Congress on Computational Methods in Applied Sciences and Engineering, 2004.

[Qattawi 2014] Qattawi, A. et al. Knowledge-based systems in sheet metal stamping: A survey. International Journal of Computer Integrated Manufacturing. 27, 2014. DOI:10.1080/0951192X.2013.834463

[Roweis 2000] Roweis, S.T. and Saul, L.K. Nonlinear Dimensionality Reduction by Locally Linear Embedding. Science, December 2000, Vol. 290, No. 22, pp 2323-2326, ISSN 0036-8075

[Shirin 2014] Shirin, M.B. and Assempour, A. Some improvements on the unfolding inverse finite element method for simulation of deep drawing process. The Internal Journal of Advanced Manufacturing Technology, 2014, Vol. 72, pp 447-456

[Tanenbaum 2000] Tanenbaum, J.B. et al. A Global Geometric Framework for Nonlinear Dimensionality Reduction. Science, December 2000, Vol. 290, No. 22, pp 2319-2323, ISSN 0036-8075

[Teskova 2005] Teskova, L. Linear algebra. Pilsen: ZCU in Pilsen, 2005. ISBN 80-7043-413-9 (in Czech)

[van der Maaten 2008] van der Maaten, L.J.P and Hinton, G. Visualizing Data using t-SNE. Journal of Machine Learning Research, 2008, Vol. 9, pp 2579-2605

[Wang 2012] Wang, J. Geometric Structure of High-Dimensional Data and Dimensionality Reduction. Beijing: Higher Education Press, 2012. ISBN 978-7-04-031704-6

[Zhang 2006] Zhang, Z. and Wang, J. MLLE: Modified Locally Linear Embedding Using Multiple Weights. Advances in Neural Information Processing Systems, January 2006, Vol. 19, pp 1593-1600

[Zienkiewicz 2005] Zienkiewicz, O.C. et al. The Finite Element Method: Its Basis and Fundamentals. Elsevier Science, 2005. ISBN 978-0-08-047277-5

CONTACTS:

Ing. Jaromir Kaspar
Advanced simulations, Innovation Department, Mubea, spol. s.r.o.
Za Dalnici 510, 267 53 Zebrak, Czech Republic
tel. +420 778 203 443, e-mail: Jaromir.Kaspar@mubea.com

Ing. Marcel Svagr
University of West Bohemia in Pilsen, RTI - Regional Technological Institute, Faculty of Mechanical Engineering
Univerzitni 22, Pilsen, 306 14, Czech Republic
tel.: +420 377 63 8299, e-mail: svagrm@kks.zcu.cz

Ing. Petr Bernardin, Ph.D.
University of West Bohemia in Pilsen, RTI - Regional Technological Institute, Faculty of Mechanical Engineering
Univerzitni 22, 306 14 Pilsen, Czech Republic,
tel.: +420 377 63 8263, e-mail: berny@kks.zcu.cz

prof. Ing. Vaclava Lasova, Ph.D.
University of West Bohemia in Pilsen, RTI - Regional Technological Institute, Faculty of Mechanical Engineering
Univerzitni 22, 306 14 Pilsen, Czech Republic,
tel.: +420 377 63 8264, e-mail: lasova@rti.zcu.cz

Ing. Otomar Sedivy, Ph.D.,
Head of Innovation Department, Innovation Department, Mubea, spol. s.r.o.
Za Dalnici 510, 267 53 Zebrak, Czech Republic
tel.: +420 737 366 879, e-mail: otomar.sedivy@mubea.com